Superficies y Vacío ***25(4)*** *234-239, diciembre de 2012*

Modelling of GaAsP/InGaAs/GaAs strain-balanced multiple-quantum well solar cells

Cabrera C. I.
Department of Physics, University of Pinar del Río
Martí 270, 20100 Pinar del Río, Cuba

Rimada J. C.
Solar cell laboratory, Institute of Materials Science and Technology (IMRE), University of Havana
Zapata y G, 10400 La Habana, Cuba

Hernández L.
Faculty of Physics. University of Havana. Colina Universitaria
10400 La Habana, Cuba

Contreras-Solorio D. A. *
Academic Unit of Physics, Autonomous University of Zacatecas
Calzada Solidaridad y Paseo La Bufa S/N, 98060
Zacatecas, Zac., México
(Recibido: 28 de septiembre de 2012; Aceptado: 30 de noviembre de 2012)

A design of de GaAsP/InGaAs/GaAs solar cell is presented that allows to model high efficiency devices. The stress, tensile and compressive, are considered in order to compute the electron and hole dispersion relation E(k) in conduction and valence band. Similarly, the optical transitions in quantum well and barriers were evaluated to calculate the quantum internal efficiency and the photocurrent. GaAsP/InGaAs/GaAs solar cell is optimized to reach the maximum performance by means of J-V relation. Our model was used to determine the highest efficiencies for cells containing quantum wells under varying degrees of strain, showing that cells with strained quantum wells achieve high efficiencies.

Keywords: Quantum well; Strain in solids; Solar cell; Conversion efficiency; Modelling

1. Introduction

The use of quantum wells to improve solar cell efficiencies was initially proposed by Barnham and Duggan [1]. The multiple quantum well solar cell (MQWSC) consists in that a number of quantum wells are incorporated in the intrinsic region of a p-i-n cell of wider bandgap (barrier or host) semiconductor to improve the spectral response of the cell in the energy region below the absorption edge of host material. The purpose of this design is that the wells absorb additional photons rising the short-circuit current. Under solar radiation, the drop in open circuit voltage (Voc) due to the inclusion of lower band-gap material can be overcompensated by the increased short-circuit current (Jsc) due to the extra photo-current from the quantum wells. Photo-generated carriers can escape from the quantum well or superlattice with near unity efficiency via a thermally-assisted tunneling process in presence of an electric field. Quantum well solar cells can achieve optimal band-gaps for the highest single-junction efficiencies due to the tunability of the quantum well thickness and composition.

GaAs solar cells currently hold the world efficiency record for single junction photovoltaic cells. The enhancement of GaAs cell efficiency is therefore important in improving solar cell performance, and then to include quantum wells in GaAs, as semiconductor host, would be the best option. However, the lattice mismatch places an upper limit on the number of quantum wells that can be accommodated before strain relaxation takes place, compromising the open circuit voltage. The first intention was to include strained GaAs/InGaAs QWSC, but they have not possessed sufficient QW absorption to increase the J_{SC} to overcome the loss in V_{OC} resulting from dislocations [2].

Other approach more successful has been to include strain-balanced GaAsP/InGaAs multiple quantum wells in the intrinsic region [3-5]. The GaAsP/InGaAs MQW strain-balanced cell (SB-QWSC) has shown an extraordinary performance for the MQW cell design, achieving 27% efficiency at 320 suns concentration [6]. Moreover, the SB-QWSC runs ahead for high-concentration triple-junction cells over the more conventional metamorphic approach. These include: the absence of dislocations [7], radiative dominance of the dark-current at high concentration and hence the possibility of radiative recycling to enhance efficiency [8], and the ability to optimize the middle cell absorption edge for different spectral conditions [9]. Possibilities exist for optimizing the structure and enhancing the efficiency of existing tandem cells.

An experimental optimization of these devices is very expensive and time-consuming. Recently, a semiempirical simulation model that is capable of predicting the external

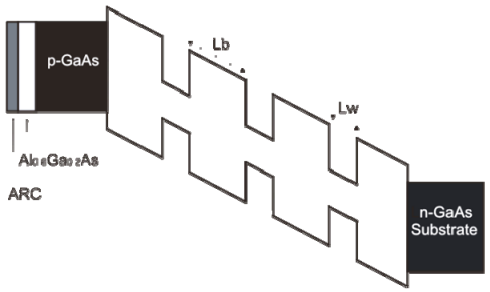

Figure 1. The band-structure of the strain-balanced quantum well solar cell. QW layers are incorporated into the i-region of a p-i-n cell.

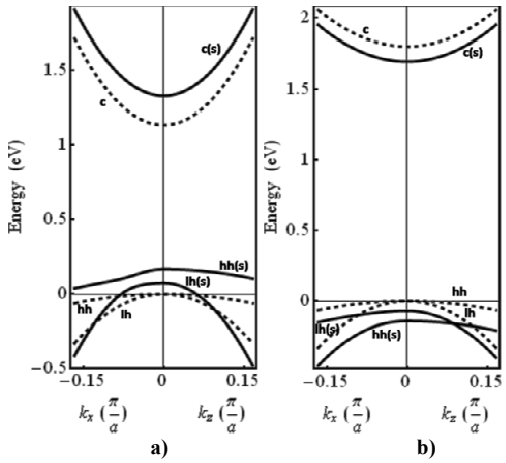

Figure 2. Energy versus wave vector diagram around of the first Brillouin zone center. LH(T) and HH(T) are strain light and heavy hole bands, respectively. (a) $In_{0.2}Ga_{0.8}As$, ε_{xx}= -0.014; ε_{zz}= 0.013. (b)$GaAs_{0.7}P_{0.3}$, ε_{xx}= 0.019; ε_{zz}= -0.010.

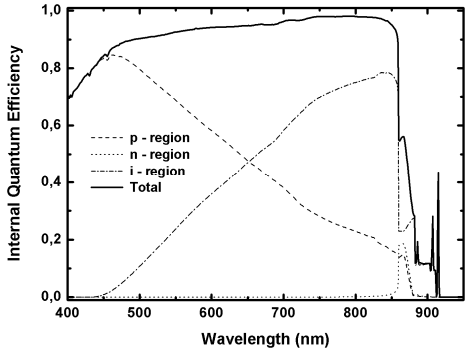

Figure 3. Modeled quantum efficiency versus wavelength for a $GaAs_{0.96}P_{0.04}/In_{0.09}Ga_{0.91}As$/GaAs SBQWSC.

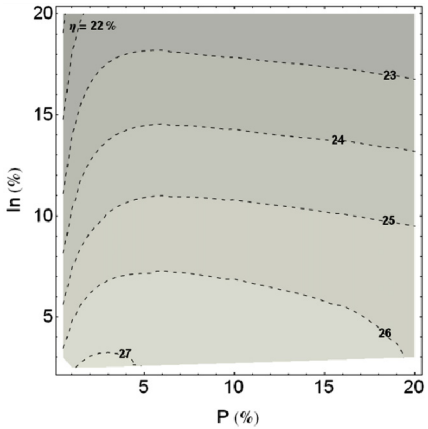

Figure 4. Contour plot for conversion efficiency versus In and P compositions. L_W = 15 nm, and N_W = 20.

quantum efficiency of SB-QWSC has been reported [10]. However, this model does not account for the strain effect, therefore the bandgaps of the materials were modified using an additional fitting parameter, reflecting this energy shift.

For this reason, an accurate modeling of a GaAsP/InGaAs/GaAs solar cell is presented here, showing that high performance devices are achievable. Tensile and compressive stresses are rigorously calculated in order to compute the electron and hole dispersion relation E(k) in conduction and valence bands. Similarly, the optical transitions in quantum well and barriers as a function of tensile and compressive stresses were evaluated without fitting parameters to calculate the quantum internal efficiency, dark current and the photocurrent and, to compare them with experimental data. The GaAsP/InGaAs/GaAs solar cell is optimized to reach the maximum performance by evaluating the current-voltage curves under illumination. Our model was used to determine the highest efficiencies for cells containing quantum wells under varying degrees of strain but it could also allow optimizing the photocurrent or the open circuit voltage in a triple-junction concentrator cell based on a SB-QWSC middle cell.

2. J-V characteristic for multiple quantum well solar cells

In this paper, we made the common assumptions of homogeneous composition in doped and intrinsic layers, the depletion approximation in the space-charge region, and total photogenerated carrier collection.

The quantum efficiency (QE) and short circuit current for a given spectrum was initially modelled. Transport and Poisson equations were used to compute the quantum efficiency in the charge-neutral layers. The fit to the QE determines the recombination characteristics independently in charge neutral and space-charge regions. This determines the radiative and non-radiative recombination currents in these regions as a function of applied bias. The overall photocurrent is simply expressed in terms of superposition, adding photocurrent to the dark current in order to ascertain the light current characteristic. At the same time, we assumed an equal carrier temperature in all regions.

A MQW solar cell with N_W wells each of length L_W in the intrinsic region of length W with barrier band gap Eg_B and well band gap Eg_W was studied in a previous work [11]. The p and n regions are uniform and symmetrically doped. Under the above mentioned assumptions, the current–voltage relation of the MQW cell is given by:

$$J = J_0\left(1 + r_R\beta\right)\left[\exp\left(\frac{qV}{kT} - 1\right)\right] + \alpha r_{NR}\left[\exp\left(\frac{qV}{2kT}\right) - 1\right] - J_{PH} \qquad (1)$$

where q is the electron charge, V is the terminal voltage, kT is the thermal energy, $\alpha = qWA_B n_{iB}$ and $\beta = \frac{qWB_B n_{iB}^2}{J_0}$ are parameters defined by Anderson [12], J_0 is the reverse saturation current density, A_B is the non radiative coefficient, B_B is the barrier recombination coefficient, n_{iB} is the equilibrium intrinsic carrier concentration for the barrier material, r_R and r_{NR} are the radiative enhancement ratio and non radiative enhancement ratio respectively, and represent the radiative and non radiative recombination increment in the net intrinsic region, due to the insertion of the quantum wells. These parameters are given by the following expressions:

$$r_R = 1 + f_W\left[\gamma_B \gamma_{DOS}^2 \exp\left(\frac{\Delta E}{kT}\right) - 1\right] \quad (2)$$

$$r_{NR} = 1 + f_W\left[\gamma_A \gamma_{DOS} \exp\left(\frac{\Delta E}{2kT}\right) - 1\right] \quad (3)$$

where $\Delta E = Eg_B - Eg_W$, f_W is the fraction of the intrinsic region volume replaced by quantum well material, $\gamma_{DOS} = g_W/g_B$ is the density of states enhancement factor, with g_W and g_B as the effective volume densities of states for the wells and barriers. The photocurrent J_{PH} is calculated from the quantum efficiency of the cell. The p-region and n-region contribution to quantum efficiency was classically evaluated solving the carrier transport equations at room temperature within the minority carrier and depletion approximations. The contribution of photo-generated carriers in the intrinsic region to QE values is calculated by the expression:

$$QE_i(\lambda) = \left[1 - R(\lambda)\right] \exp\left\{-\sum_j \alpha_j z_j\right\} \left[1 - \exp\left\{-\alpha_p x_{wp} - \alpha_n x_{wn} - \alpha_i W\right\}\right] \quad (4)$$

where $R(\lambda)$ is the surface reflectivity spectrum of the antireflection coating. The first exponential factor is due to the attenuation of light in the precedent layers of the cell, α_j and z_j are the absorption coefficient and the width of the precedent layers, respectively, $\alpha_{p,n}(\lambda)$ is the absorption coefficient in p or n-region and $x_{wp,wn}$ is the depletion region width corresponding to p or n-region, and α_j is given by the following expression:

$$\alpha_i(\lambda) W = \alpha_B(\lambda) W_B + \alpha_W(\lambda) W_W + \alpha_{QW}(\lambda) \Lambda N_w \quad (5)$$

where $\alpha_B(\lambda)$ is the absorption coefficient of the bulk barrier material, $\alpha_W(\lambda)$ is the absorption coefficient of the bulk well material, W the depletion region width, W_B and W_W are the barrier and well width, $\alpha_{QW}(\lambda)$is the well absorption coefficient, N_w is the quantum well number and Λ is the ''quantum thickness of the heterostructure''.

Following Bastard [13], we calculate the density of states for the single quantum well within the envelope function approximation. When mixing between light and heavy valence sub-bands is neglected, the well absorption coefficient can be calculated as follows:

$$\alpha_{QW}(\lambda) = \sum_{n,m} \alpha_{e_n - hh_m}(\lambda) + \sum_{n,m} \alpha_{e_n - lh_m}(\lambda) \quad (6)$$

where $\Sigma\alpha_{e_n - hh_m}(\lambda)$ and $\Sigma\alpha_{e_n - lh_m}(\lambda)$ are the absorption coefficients due to electron-heavy hole and electron-light hole transitions to conduction band, respectively. The long wavelength region the exciton absorption is considered in the calculation and the exciton binding energies are analytically evaluated in the framework of fractional–dimensional space [14]. Once the total QE is calculated the photocurrent is determined by integration:

$$J_{PH} = q\int_{\lambda_1}^{\lambda_2} F(\lambda) QE_{TOTAL}(\lambda) d\lambda \quad (7)$$

where λ_1 and λ_2 are limits of the taken solar spectrum $F(\lambda)$, using the air mass coefficient AM1.5 [15], which defines the direct optical path length through the Earth's atmosphere, expressed as a ratio relative to the path length vertically upwards. Then, Eq. (1) is completely determined and conversion efficiency (η) can be evaluated.

3. Strain-balanced quantum well solar cells

Strain-balanced multi-quantum well solar cells (SB-QWSC) were proposed as a novel approach to increase the efficiency of conventional GaAs solar cells by extending the spectral response. The SB-QWSC is a GaAs p-i-n solar cell with quantum well layers incorporated into the i-region with InGaAs as well material and GaAsP as barrier material. Figure 1 shows the band-structure of the GaAsP/InGaAs/GaAs SB-QWSC which was modeled. The compressive strain in the InGaAs QW is matched by tensile strain in GaAsP barriers, overcoming the lattice-mismatch limitation. The GaAsP and InGaAs layer widths were chosen to ensure the average lattice parameter across the *i*-region was equal to that of GaAs. Elastic constants were considered to evaluate the tensile and compressive stresses in GaAsP and InGaAs layers. Thus, if L_b is the barrier thickness, L_w is the well thickness, $a_{\mathrm{GaAs1\text{-}y\ Py}}$ and $a_{\mathrm{InxGa1\text{-}xAs}}$ are the respective well and barrier lattice constants; we define

$$a_{GaAs} \equiv \langle a \rangle = \frac{L_b a_{GaAs_{1-y}P_y} + L_w a_{In_xGa_{1-x}As}}{L_b + L_w} \quad (8)$$

The epitaxial layers grow on a substrate with slightly mismatched lattice constant and the layer thickness is below some critical value, a high quality strained epitaxial layer can be grown without dislocation. The InGaAs wells are compressively strained and the width is chosen to be

below the critical thickness. The barriers are in tensile strain and the widths and compositions of wells and barriers are adjusted to ensure zero-stress at interfaces.

The *p* and *n* regions were designed to 200 and 500 nm in width, respectively, and a 40 nm $Al_{0.8}Ga_{0.2}As$ window layer was incorporated into the *p* region to reduce front surface recombination. The hole and electron concentrations are p = 10^{18} cm^{-3} and n = 10^{18} cm^{-3}, respectively. The antireflection coating (ARC) is a 70 nm MgF:SiN layer. A passivation layer in the solar cell rear with 200 cm/s surface recombination velocity was assumed.

The electric field and stress, tensile and compressive, are considered in order to compute J-V relation and this way, to design high efficiency GaAsP/InGaAs/GaAs solar cell. For this purpose, the optical transitions in quantum well and barriers were evaluated to calculate the quantum internal efficiency and the photocurrent. The highest efficiencies for cells containing quantum wells under varying degrees of strain were determined, showing that cells with strained quantum wells achieve high efficiencies.

4. Strain effects on photon absorption in the *i*-region

Below the critical thickness, almost all the strain is incorporated in the layer which is then under biaxial stress such that its in-plane lattice constant equals the substrate lattice constant. This type of coherently strained layer is called pseudomorphic growth. Biaxial strain can only be achieved on the nano-scale, giving nano-structured solar cells a fundamental advantage over bulk semi-conductor solar cells. The changes of band structure of the layer under strain have significant effects on the SB-QWSC.

The growth of strained GaAsP and InGaAs layers allows a wider choice of P and In compositions to fit the energy levels in the quantum wells. Thus, the balanced strain between GaAsP and InGaAs layers is also designed as an extra parameter to tailor the layer materials and the SB-QWSC performance.

For unstrained bulk material, the heavy hole (*hh*) and light hole (*lh*) bands at the top of the valence band are degenerate at the Brillouin zone centre. Biaxial strain modifies the lattice size and the symmetry, which in turn changes the quantum well energy levels and lifts the degeneracy of the electronic bands. Under compressive strain, bottom energy of the conduction band is displaced to higher energy and the QW valence band splits, with the lh level moving further from the conduction band suppressing the *lh* transition [16]. On the contrary, under tensile strain the GaAsP band gap is reduced. Consequently, when the In an P compositions are varied, the strains in the barrier and well layers modify absorption threshold in both layers.

The lattice constant a_j of the epitaxial layer in the growth interface is forced to be equal to the lattice constant of the substrate a_i. Therefore, there is in-plane strain ε_{ij}, defined by:

$$\varepsilon_{ij} = \frac{a_j - a_i}{a_j} = \frac{\Delta a_i}{a_j} \tag{9}$$

where *i, j = x, y, z*. These values hence can be different in each direction. The force perpendicular to the interface is zero. However, the lattice constant along this direction is changed due to the Poisson effect. If a compressive stress is applied, the in-plane constant is forced to shrink and the perpendicular lattice constant will grow or vice versa.

For biaxial stress in (001) plane in the strain quantum wells, the ε_{ij} values along [001] direction are $\varepsilon_{xx} = \varepsilon_{yy}$ y $\varepsilon_{xx} = \varepsilon_{yy} \neq \varepsilon_{zz}$. Both stress components are related with C_{11} and C_{12} elastic constants by the expression [17]:

$$\varepsilon_{zz} = -2\frac{C_{12}}{C_{11}}\varepsilon_{xx} \tag{10}$$

with $\varepsilon_{xx} = \frac{a_{st} - a_0}{a_0}$ where a_{st} and a_0 are strain and without strain lattice constants, respectively. The stress causes changes in the band borders in Γ point, which are given by reference [17]:

$$E_{hh}\left(\vec{k} = 0\right) = E_{hh}^0 = E_v^0 - P_\varepsilon - Q_\varepsilon \tag{11}$$

$$E_{lh}\left(\vec{k} = 0\right) = E_{lh}^0 = E_v^0 - P_\varepsilon + Q_\varepsilon \tag{12}$$

where $\boldsymbol{E_{hh}^0}$ and $\boldsymbol{E_{lh}^0}$ are the new energy level values under stress for heavy and light holes, respectively, $\boldsymbol{E_v^0}$ is the valence band top and,

$$P_\varepsilon = -a_v\left(\varepsilon_{xx} + \varepsilon_{yy} + \varepsilon_{zz}\right) \tag{13}$$

$$Q_\varepsilon = -\frac{b}{2}\left(\varepsilon_{xx} + \varepsilon_{yy} - 2\varepsilon_{zz}\right) \tag{14}$$

The conduction band bottom is given by:

$$E_c(\vec{k} = 0) = E_c^0 = E_v^0 + E_g + a_c\left(\varepsilon_{xx} + \varepsilon_{yy} + \varepsilon_{zz}\right) \tag{15}$$

where E_g is the band gap, a_v and a_c are so-called hydrostatic deformation potentials and b is the shear deformation potential. The separation of the total hydrostatic deformation potential in conduction (a_c) and valence band (a_v) contributions is important at heterointerfaces. Varying the wave vector $\vec{k}$ values, the E versus k diagram is obtained for both materials, InGaAs and GaAsP, which are shown in figure 2. Note that due to stress, the $In_{0.2}Ga_{0.8}As$ layer undergoes a 121 meV band gap increment, while $GaAs_{0.7}P_{0.3}$ layer a decrease of 176 meV is obtained. When the In and P compositions as well as their layer widths are varied, such that the condition given by equation (8) is satisfied, the stress is changed in the well and barrier layers, causing in both films a deviation in the absorption threshold.

5. Electron and hole energy level computation in strain quantum wells

The envelope function approximation is here assumed to compute QW energy levels in CB. The electron energy E_c and wave function ψ_c can be calculated with the effective mass approximation. Then, the motion of the conduction band electron in the QW is described by Schrödinger equation.

In order to determine the QW energy levels in the *hh* and *lh* bands under varying compressive strain a 4x4 *k.p* Kohn-Luttinger Hamiltonian H^{ε}_{KL} was used:

$$H^{\varepsilon}_{KL} = H_{KL} + H^{\varepsilon} \tag{16}$$

where $\boldsymbol{H_{KL}}$ is the Kohn-Luttinger Hamiltonian without stress and $\boldsymbol{H^{\varepsilon}}$ is the stress Hamiltonian that for epilayers grown in (001) direction is given by [18]:

$$H^{\varepsilon} = \begin{bmatrix} H^{\varepsilon}_{hh} & 0 & 0 & 0 \\ 0 & H^{\varepsilon}_{lh} & 0 & 0 \\ 0 & 0 & H^{\varepsilon}_{lh} & 0 \\ 0 & 0 & 0 & H^{\varepsilon}_{hh} \end{bmatrix} \tag{17}$$

with

$$H^{\varepsilon}_{hh} = a_v(2\varepsilon_{xx} + \varepsilon_{zz}) - b(\varepsilon_{xx} - \varepsilon_{zz}) \tag{18}$$

$$H^{\varepsilon}_{hh} = a_v(2\varepsilon_{xx} + \varepsilon_{zz}) - b(\varepsilon_{xx} - \varepsilon_{zz}) - b^2\frac{(\varepsilon_{xx} - \varepsilon_{zz})^2}{\Delta_{SO}} \tag{19}$$

where $\boldsymbol{\Delta_{SO}}$ is the spin-orbit splitting of the VB at Γ point. The biaxial strain, in well and barriers layers, lifts the degeneracy in the valence band such that it is possible to considerer independently the hh and lh bands. Under above approximations, the QW energy levels for *hh* and *lh* bands are given by:

$$\left[H^{\varepsilon}_{KL} - IE\right]\Psi = 0 \tag{20}$$

where $\Psi = \left(\psi^{\uparrow}_{hh} \quad \psi^{\uparrow}_{lh} \quad \psi^{\downarrow}_{lh} \quad \psi^{\downarrow}_{hh}\right)^T$, $\psi^{\uparrow\downarrow}_{hh}$ and $\psi^{\uparrow\downarrow}_{lh}$ are the envelope functions with spin direction (up↑ and down↓) and *I* is the unity matrix. The Schrödinger equation corresponding to H^{ε}_{KL} Hamiltonian is not separated so it is assumed that the "off-diagonal" terms are small enough that they can be neglected. With this assumption the Schrödinger equation becomes separable:

$$\left[-\frac{\hbar^2}{2m_0}(\gamma_1 - 2\gamma_2)\frac{d^2}{dz^2} + V(z) + H^{\varepsilon}_{hh} - E_{hh}\right]\psi^{\uparrow\downarrow}_{hh}(z) = 0 \tag{21}$$

$$\left[-\frac{\hbar^2}{2m_0}(\gamma_1 - 2\gamma_2)\frac{d^2}{dz^2} + V(z) + H^{\varepsilon}_{lh} - E_{lh}\right]\psi^{\uparrow\downarrow}_{lh}(z) = 0 \tag{22}$$

The equations (21) and (22) are solved in barrier and well regions with the corresponding *V(z)* potential and Konh-Luttinger parameter ($\gamma_i$and γ_2) values in each layer in order to compute E_c, E_{hh} and E_{lh}. Once found the energy level values, the optical transitions were calculated by Fermi's golden rule. Later, equation (6) was evaluated to determine the absorption in the quantum wells and thus to calculate *QE*.

6. Electric field effects on photon absorption in the *i*-region

In the SBMQWSC, the net positive and negative charges in the *n*- and *p*-regions induce an electric field *F*(z) in *i*-region perpendicular to QW interfaces which causes a change in the potential profile to *V(z) – qF(z)*. In presence of the electric field an alignment between the MQW energy levels is not achievable, so that for any barrier thickness that satisfies the equation (8), the different quantum wells are independent of each other and there is no coupling between neighboring quantum wells. The confined state energy levels shift under electric field (Stark effect) decreasing the absorption threshold. Using the Schrödinger equation, the energy shifts can be calculated by perturbation method.

7. Results and discussion

The quantum efficiency as a function of wavelength was computed by means of eq. (4). Figure 3 shows spectral response of a 15 well $GaAs_{0.96}P_{0.04}/In_{0.09}Ga_{0.91}As/GaAs$ SBMQWSC. The QWs extend absorption from GaAs bulk band-gap (λ = 890 nm) to threshold energy determined by the confinement energy. The extra absorption is shown in figure 3, at wavelengths in excess of the GaAs band gap, the cell absorption is extended to 920nm, leading an increment in the short circuit current. The GaAsP barriers are responsible for the small drop in quantum efficiency at their absorption edge (835 nm). The modeled QE(λ) is very similar to experimental spectral response reported by Mazzer et al. [4] and the coincidence is not total because the cell parameters are slightly different.

The strain and electric field effects that do not explicitly show in eq. (1) were considered to evaluate the J-V characteristic. When the In and P compositions are varied or their width layer are changed, the generated strain modifies the absorption threshold. In a QW system, some splitting of the confined valence band levels takes place due to the differences in effective mass. This splitting can be greatly enhanced if the QW is strained. Similarly, when the depletion region width *W* is changed, the electric field variation also modifies the absorption threshold.

The dependence of conversion efficiency on In and P composition is examined in figure 4 for L_W = 15 nm and N_W=20, the L_b values are varied, in order to satisfy strain-balanced condition (eq. 8). The white region corresponds to In and P compositions for which the energy transitions between QW levels are larger than GaAs band gap. These optical transitions were not considered in the calculations.

Figure 4 shows that the In fraction influences more in the conversion efficiency than P fraction. Enlarging In composition in the QW, the layer barrier width must be increased to settle down strain-balanced condition, leading to larger radiative a no-radiative recombination in the barrier region that increases the leakage current. Otherwise, with P fraction variation, the recombination process does not significantly change due to a slightly reduction of the barrier width. Besides this behavior, the P fraction increment originates enhancing of absorption threshold in the strained barrier that reduces the absorbed photon number of the solar spectrum such that the photocurrent decreases slightly. We can conclude that the In composition is the critical factor in the SB-QWSC performance. Additionally, note from figure 4, that until 3% In and 5% P compositions, a conversion efficiency so high as 27 % is reached.

8. Conclusions

The strain-balanced multiple quantum well solar cells show a high conversion efficiency that it makes very attractive for space applications. The eq. (1) was extended to incorporate the strain and electric field effects on absorption of the photons in i-region. The conversion efficiency was optimized as a function of quantum well width, In and P compositions. The maximum performance value was obtained for In, x = 0.02, P, y = 0.04 and L_w = 18 nm. High conversion efficiencies are reached for shallow wells, small In and P compositions, where radiative recombination is very low. However, for deep wells, reverse saturation currents are dominated by recombination in the quantum wells and then the conversion efficiency falls. The model also allows optimizing other SB-QWSC parameters to achieve high performance, such as N_W, W, doping and width of emitter and base regions. It was shown that cells with highly strained quantum wells achieve high efficiencies.

Acknowledgments

This work has been partially supported by PROMEP, COZCYT and CONACYT, Mexico.

References

[1] K. W. J. Barnham and C. J. Duggan, J. Appl. Phys. **67** 3490 (1990).
[2] P. R. Griffin, J. Barnes, K. W. J. Barnham, G. Haarpaintner, M. Mazzer and C. Zanotti-Fregonara, E. Grünbaum, C. Olson and C. Rohr, J. P. R. David, J. S. Roberts, R. Grey, and M. A. Pate, J. Appl. Phys. **80**, 10 (1996).
[3] N. J. Ekins-Daukes, K. W. J. Barnham, J. P. Connolly, J. S. Roberts, J. C. Clark, G. Hill, M. Mazzer. Appl. Phys. Lett. **75** 495 (1999).
[4] M. Mazzer, K. W. J. Barnham, I. M. Ballard, A. Bessiere, A. Ioannides, D. C. Johnson, M. C. Lynch, T. N. D. Tibbits, J. S. Roberts, G. Hill and C. Calder, Thin Solid Films **511**, 76 (2006).
[5] J. G. J. Adams, W. Elder, P. Stavrinou, K. W. J. Barnham. 24th European Photovoltaic Solar Energy Conference, September 21-25, 2009, Hamburg, Germany.
[6] D. C. Johnson, I. Ballard, K. W. J. Barnham, M. Mazzer, T. N. D. Tibbits, J. Roberts, G. Hill, and C. Calder. 4th World Conference on Photovoltaic Energy Conversion, pages 26-31, 2006.
[7] N. J. Ekins-Daukes, J. M. Barnes, K.W. J. Barnham, J. P. Connolly, M. Mazzer, J. C. Clark, R. Grey, G. Hill, M. A. Pate, J. S. Roberts, Sol. Energ. Mat. Sol. C., **68**, 71 (2001).
[8] D. C. Johnson, I. M. Ballard, K.W. J. Barnham, J. P. Connolly, M. Mazzer, A. Bessière, C. Calder, G. Hill and J. S. Roberts, Appl. Phys. Lett, **90**, 213505 (2007).
[9] B. C. Browne, A. Ioannides, J. P. Connolly, K. W. J. Barnham, J. S. Roberts, R. Airey, G. Hill, G. Smekens and J. V. Begin, Proceedings 33rd IEEE Photovoltaic Specialists Conference (2008), p. 144.
[10] P. Kailuweit, R. Kellenbenz, S. P. Philipps, W. Guter, A. W. Bett and F. Dimroth, J. Appl. Phys. **107**, 064317 (2010).
[11] J. C. Rimada, L. Hernandez, K.W. J. Barnham and J. P. Connolly, Phys. Status Solidi B., **242**, 1842 (2005).
[12] N. G. J. Anderson. J. Appl. Phys. **78**, 1850 (1995).
[13] G. Bastard, Wave Mechanics Applied to Semiconductor Heterostructures (Editions de Physique, Paris, 1988).
[14] H. Mathieu, P. Lefebre, and P. Christol, Phys. Rev. B, **46** 4092 (1992).
[15] ASTM G173-03 Standard Tables for Reference Solar Spectral Irradiances: Direct Normal and Hemispherical on 37 oC Tilted Surface, ASTM International. For referenced ASTM standards, visit the ASTM website hwww.astm.orgi, or contact ASTM Customer Service at service@astm.org. For Annual Book of ASTM Standards volume information, refer to the standards Document Summary page on the ASTM website.
[16] A. Khan, in: Low Dimensional Semiconductor Structures. Eds. K. Barnham and D. Vvedensky, (Cambridge, 2001) pp. 280-286.
[17] S**.** Chuang, Phys. Rev. B, **43**, 9649 (1991).
[18] J. Piprek, Semiconductor Optoelectronic Devices, (Academic Press, 2003) pp. 27-30.